OPTIMIZATION OF LINK PARAMETERS FOR A 7 DOF MANIPULATOR BASED ON WORKSPACE VOLUME AND MOTION FLEXIBILITY

Xinglei ZHANG[1, *], Chao HAN[1], Chuanxiu WU[2], Su XU[3], Yu XU[1], Wenliang ZHU[1]*, Xingqian XIE[1], Guangying ZHANG[4]

After the structural design of a 7 degree-of-freedom (DOF) manipulator is completed, it is essential to continue optimizing its link parameters. The workspace volume and motion flexibility are important kinematic indicators for evaluating the performance of the manipulator. First, the average manipulability is introduced as a global flexibility index for the manipulator, and the impact of link parameters on the workspace volume and average manipulability is analyzed. Then, with the manipulator link parameters and the absence of voids in the workspace as constraints, and the workspace volume and average manipulability as objective functions, the Particle Swarm Optimization (PSO) algorithm is applied to solve the problem. Finally, a comparative analysis of the link parameters, workspace volume, and average manipulability before and after optimization is conducted. The results show that, after optimization, the total sum of joint variables is reduced, and both the workspace volume and average manipulability are significantly improved. This indicates that the optimized manipulator has a larger workspace and more flexible in motion, further verifying the effectiveness of the link parameter optimization for the manipulator.

Key words: 7 DOF Manipulator, parameter optimization, workspace volume, motion flexibility, average manipulability.

1. Introduction

The workspace is the set of positions that the end effector of a manipulator can reach, determined by the geometric shape of the manipulator, the dimensions of the links, and the range of motion of each joint position [1]. The acquisition methods include graphical methods, analytical methods, numerical methods, etc. The graphical method involves using computers to plot the workspace of the

[1]School of Mechanical Engineering, Jiangsu Ocean University, Lianyungang, 222005, China.
2Jiangsu Suyun Medical Device Co., Ltd, Lianyungang, 222002, China.
[3]School of Innovation and Entrepreneurship, Jiangsu Ocean University, Lianyungang, 222005, China.
[4]School of Mechanical and Electrical Engineering, Weifang Engineering Vocational college, Weifang, 224051, China.
*Email: zhangxingfulove@163.com, zwliang2001@qq.com

manipulator, which is typically suitable for manipulators with fewer than 3 DOF. The analytical method uses algebraic expressions to derive the equations of the boundary surfaces of the manipulator's workspace, thereby obtaining a distribution diagram of the workspace. However, this method is computationally complex [2]. Numerical methods determine the workspace through computer simulation and numerical calculations and the Monte Carlo method is a commonly used approach. It involves randomly generating a large number of joint angle combinations and calculating the positions of the end effector through forward kinematics. The workspace is then approximated by statistically analyzing these position points [3].

After designing the mechanical arm structure, optimizing its link parameters is essential. Jing [4] analyzed and optimized the collaborative space and parameters of a 6R dual-arm service robot. Feng [5] and colleagues combined workspace analysis with structural length indicators, employing parameter optimization methods to refine the configuration and structural parameters of a picking manipulator. Yin [6] applied Dijkstra's optimization theory to maximize the workspace of a stone-carving robotic arm and conducted a motion performance analysis. Lan [7] established an optimization model with the maximum occupied area as the objective function and used genetic algorithms to optimize design parameters.

However, the workspace of the manipulator obtained by the Monte Carlo method has the disadvantage of low boundary accuracy [8]. Moreover, the workspace obtained by the Monte Carlo method is difficult to describe mathematically, which is not conducive to optimizing the link parameters when the workspace is used as the objective function.

Unreasonable link dimension design can lead to voids in the workspace, degrading motion performance. If the size of the voids in the workspace of the robotic arm is smaller than the width of the arm's links themselves, such as in the case of the UR5 robotic arm, the impact on the performance is minimal. Conversely, if the size of the voids exceeds the width of the arm's links, it can severely affect the working performance of the robotic arm. Given that the workspace cloud map obtained by the Monte Carlo method does not allow for a direct judgment of the presence of voids, one can only obtain this information by vertically stratifying the three coordinate axes to get the cloud point diagrams of each layer of the workspace. This approach’s effectiveness depends on the layer thickness, resulting in low efficiency and lack of reliability. Moreover, voids further reduce the solution accuracy for a 7-DOF manipulator’s workspace.

During the operation of a robotic arm, in addition to pursuing a larger workspace, it is also necessary to improve its flexibility as much as possible. Paul and Stevenson [9] used the determinant value of the Jacobian matrix as the objective function for flexibility and optimized the link parameters. However, this

method is only applicable when the Jacobian matrix is a square matrix. Salisbury [10] and Yu [11] proposed the definition of the matrix condition number, using it as an evaluation index for the flexibility of the robot and as the objective function for optimizing the link parameters. Mayorga et al. [12] used the maximum rate of change of the isotropic index as the objective function for link parameter optimization. Dong [13] constructed a workspace density function model, and used the distribution range of the maximum value of the workspace density function as the objective function for the flexibility of the manipulator's motion to optimize the link parameters. Zhao [14] and Li [15] used the manipulability index as the objective function for link parameter optimization to improve the flexibility of the manipulator's motion. Liang [16] optimized the scale parameters based on the global mean and fluctuation of the manipulability matrix condition number. Hu [17] constructed a multi-objective optimization index of manipulability and condition number, and obtained the optimal solution through the SGA-II algorithm. Yang [18] introduced an optimization index that maximizes the manipulability at the acceleration level during the inverse kinematics solution process of redundant manipulators. Liao [19] used a normalized manipulability as the evaluation index to optimize the configuration of Supernumerary robotic limbs as the objective function. However, the above objective functions are all optimized based on local flexibility indicators and lack reliability. In fact, many flexibility indicators can be used as objective functions, but different chosen indicators will have a certain impact on the optimization results of the link parameters of the 7 DOF manipulator.

To address the shortcomings, this paper proposes a dual-objective optimization method for the link parameters of a 7-DOF manipulator, considering both workspace volume and motion flexibility. First, the mathematical model for workspace volume calculation and the non-void condition proposed in [20] are adopted as the objective function and constraint function, respectively. The influence of each link parameter on workspace volume is systematically analyzed. Next, the effects of link parameters on motion flexibility are evaluated, with average manipulability selected as the quantitative flexibility index. Finally, the dual-objective problem is converted into a single-objective optimization problem by introducing weight coefficients and scaling factors, and the optimal link parameters are determined using the PSO algorithm.

2. Research on the influence of connecting rod parameters on workspace volume

Using a 7 DOF manipulator designed in the laboratory as an example, the 3D model and spatial coordinate system of the 7 DOF surgical manipulator are

constructed, as shown in Figure 1. The modified D-H parameters are shown in Table 1.

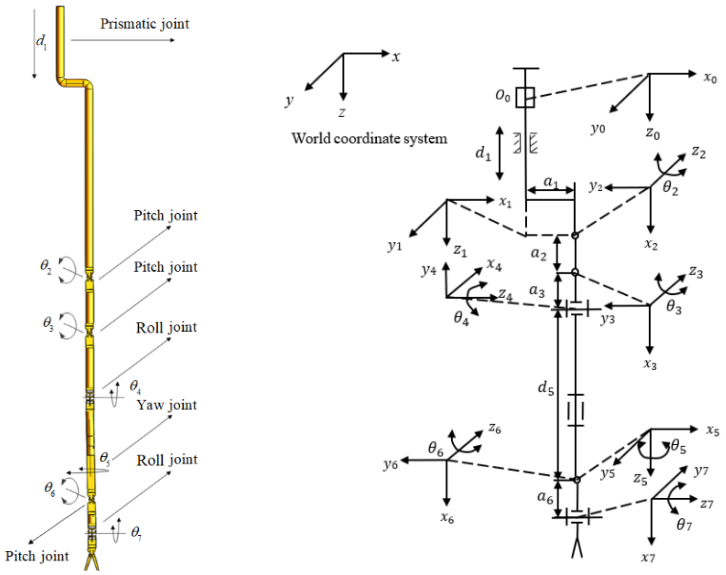

(a) The 3D model (b) The spatial coordinate system

Fig. 1. The 3D model and coordinate system of the 7 DOF manipulator

Table 1

The modified D-H parameters of the 7-DOF redundant manipulator

i	α_{i-1} (rad)	a_{i-1} (mm)	d_i (mm)	θ_i (rad)
1	0	0	d_1	0
2	$\pi/2$	a_1	0	$\theta_2\,(\pi/2)$
3	0	a_2	0	$\theta_3\,(0)$
4	$\pi/2$	a_3	0	$\theta_4\,(\pi/2)$
5	$\pi/2$	0	d_5	$\theta_5\,(\pi/2)$
6	$\pi/2$	0	0	$\theta_6\,(\pi/2)$
7	$\pi/2$	a_6	0	$\theta_7\,(0)$

Reference [20] provides the formulas for calculating the working volume of a robotic arm as follows:

$$V = \sum_{j=1}^{L} v(j) \tag{1}$$

where $v(j)=S(j)\frac{x_2-x_1}{L}$, $S(j)=\sum_{\tilde{i}=1}^{M}s(\tilde{i})$, $s(\tilde{i})=f(\tilde{i})-g(\tilde{i})$, $f(\tilde{i})=\kappa(z_{\max}^{\tilde{i}}-z_{\min}^{\tilde{i}})$, $g(\tilde{i})=\begin{cases}\kappa(z_{\tilde{i}+1}-z_{\tilde{i}}) & z_{\tilde{i}+1}-z_{\tilde{i}}>\kappa\\ 0 & z_{\tilde{i}+1}-z_{\tilde{i}}\le\kappa\end{cases}$, x_1 and x_2 are the minimum and maximum values of the robotic arm's workspace in the *x*-axis direction obtained by the Monte Carlo method. L represents the number of layers that divide the workspace perpendicular to the *x*-axis. Each layer is approximated as a thin three-dimensional body of different shapes parallel to the *y*-*o*-*z* plane. *M* represents the number of columns for rectangular segmentation of each thin three-dimensional body in each layer. In all *M* columns of rectangles, each column of rectangles is further divided into *H* layers along the *z*-axis direction, producing *H*+1 *z*-coordinate values, which are then sorted in ascending order as $z_1<z_2<\cdots z_{\tilde{i}}<z_{\tilde{i}+1}<\cdots z_{H+1}$. $z_{\tilde{i}}$ is the *z*-coordinate value of the *i*-th uniform division along the *z*-axis of each rectangular column in the layer. $z_{\max}^{\tilde{i}}$ and $z_{\min}^{\tilde{i}}$ are the maximum and minimum values along the *z*-axis direction of each thin three-dimensional body, respectively. κ is associated with the transverse dimension of the designed robotic manipulator's connecting rod.

Additionally, reference [20] provides the formulas for the constraints for a void-free workspace of a robotic arm as follows:

$$\left|d_5-a_6\right|\le\left|a_2+a_3\right|\le\left|d_5+a_6\right| \tag{2}$$

The parameters of a robotic arm's links include link dimensions, link offsets, and joint position ranges. This section takes the manipulator shown in Figure 1 (a) as an example to analyze the impact of link parameters on the working volume and provide a basis for the optimization of link parameters in subsequent designs. The analysis of link dimensions and link offsets is premised on the condition that they are varied individually within a certain range while all other lengths remain constant. Links $a_1=20\text{mm}$, $a_2=50\text{mm}$, $a_3=50\text{mm}$, $d_5=100\text{mm}$, and $a_6=30\text{mm}$ are selected as the baseline link parameters to analyze the impact of link dimensions, link offsets, and joint position ranges on the working volume.

2.1 Analysis of the impact of link dimensions and link offsets on the workspace volume

Nineteen values are selected around each basic parameter, with adjacent values differing by 2.5mm. This paper sets $N = 200000$ (where N is the number of joints randomly generated within the range of motion for each joint when using the Monte Carlo method to calculate the workspace), $L = 20$, $M = 10$. Due to the prismatic joint at O_0, it is obvious that the rigid arm a_1 cannot change the working volume. The resulting working volume is the outcome under the joint position range shown in Table 1. The changes in the working volume as each link dimension and link offset vary from low to high are depicted in Fig. 2.

Observing Figure 2, the following conclusions are drawn: (1) When a_1 changes, V of the manipulator fluctuates around $3.6625\times10^7\,\mathrm{mm}^3$. The slight fluctuations are due to the randomness of the joint position points in the Monte Carlo method for calculating the working volume. Therefore, this parameter does not affect V. (2) At $a_3 = 50$, a local maximum appears. The reason for this may be that certain combinations of link lengths and joint angles cause some parts of the manipulator to interfere with each other, restricting the movement of the end effector in certain directions. It could also be that the manipulator requires greater force or torque to move in certain directions, thereby reducing its flexibility and efficiency. However, from a global perspective, increasing the lengths of a_2, a_3, d_5, and a_6 all increase V, but compared to a_2 and a_3, d_5 and a_6 have a greater slope for increasing V. Among them, the 5th joint is a rotating joint, and from Figure 2, it is known that d_5 is the length between joint 4 and joint 6, which can be appropriately larger; considering that the 7th joint is connected to the end-effector, to avoid excessive position changes of the end-effector when its posture changes, the length of a_6 should not be too large. (3) The slopes of change for a_2 and a_3 are slightly different, with the former corresponding to V about

$0.3\times10^7\,\mathrm{mm}^3$ larger than the latter, indicating that a_2 has a slightly greater impact on V than a_3.

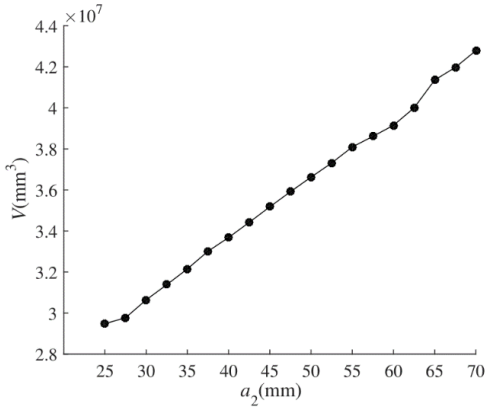

(a) The influence pattern of a_2 on V.

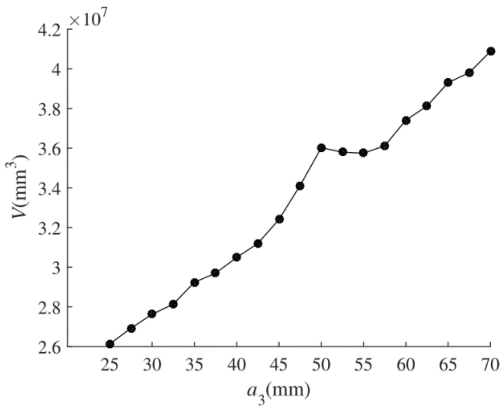

(b) The influence pattern of a_3 on V.

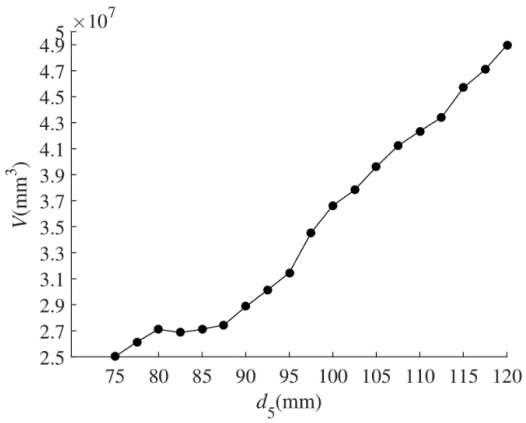

(c) The influence pattern of d_5 on V.

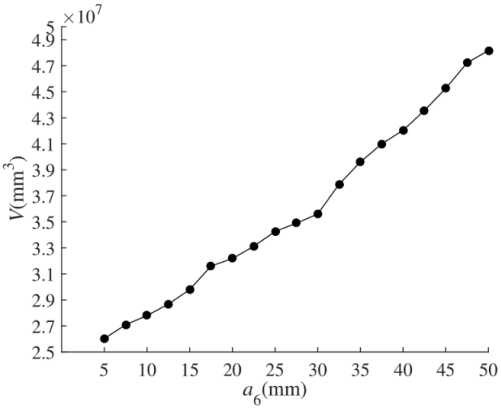

(d) The influence pattern of a_6 on V.

Fig. 2 Influence of connecting rod size and connecting rod offset on V

2.2 Analysis of the impact of joint position range on the workspace volume

Each joint position range is changed one by one while the other joint position ranges remain constant. The changes in V as each joint position range varies are shown in Figure 3.

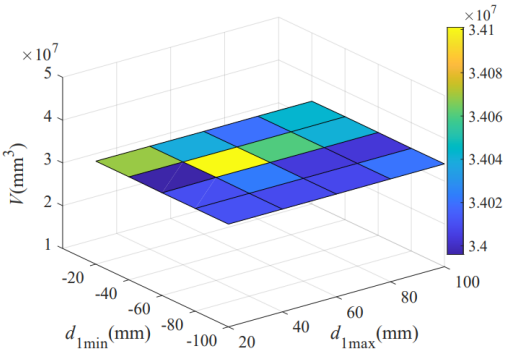

(a) The influence pattern of d_1 on V.

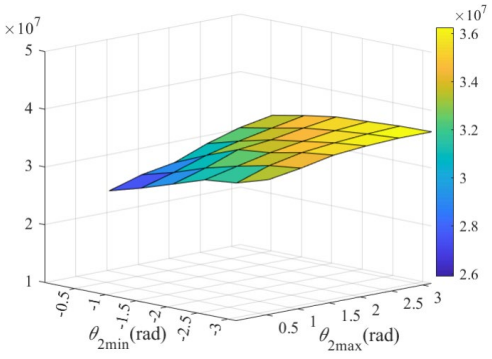

(b) The influence pattern of θ_2 on V.

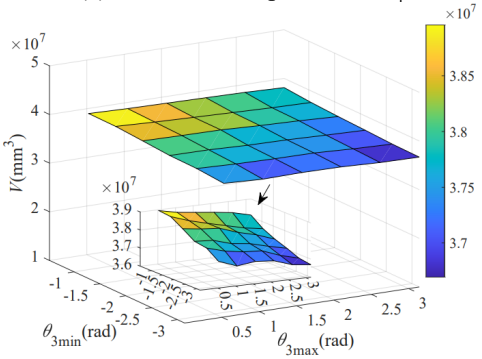

(c) The influence pattern of θ_3 on V.

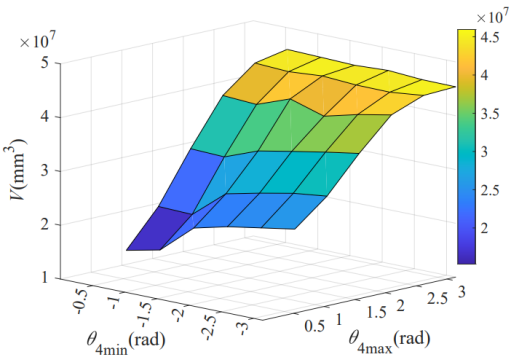

(d) The influence pattern of θ_4 on V.

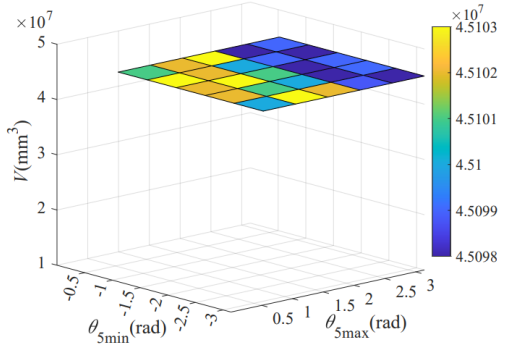

(e) The influence pattern of θ_5 on V.

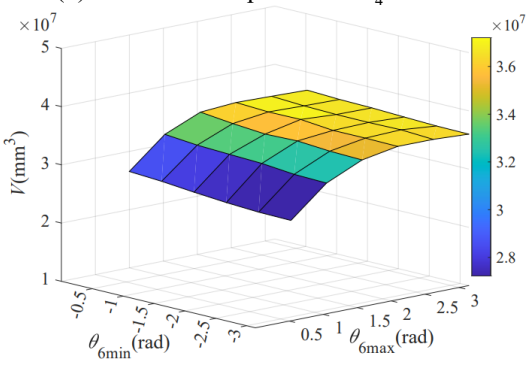

(f) The influence pattern of θ_6 on V.

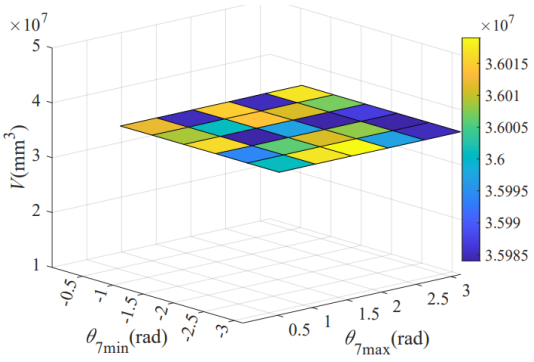

(g) The influence pattern of θ_7 on V.

Fig. 3 Influence of range variation of joint position on V.

Observing Figure 3, the following conclusions are drawn: (1) When the range of the mobile joint d_1 changes, V of the robotic arm fluctuates around $3.405\times10^7\,\mathrm{mm}^3$. When the ranges of the rotating joints θ_5 and θ_7 change, V of the manipulator fluctuates around $4.51\times10^7\,\mathrm{mm}^3$ and $3.6\times10^7\,\mathrm{mm}^3$, respectively. That is, the changes in the position ranges of these three joints have a small impact on V, and the reason for the small fluctuations is the randomness of the position points when using the Monte Carlo method to calculate V. (2) When the ranges of joints θ_2, θ_4, and θ_6 decrease, V tends to decrease, with $V_{\max}$ occurring at $\theta_2 \in [-\pi, \pi]$, $\theta_4 \in [-2\pi/3, \pi]$, and $\theta_6 \in [-\pi/6, 2\pi/3]$, respectively. (3) When the range of joint θ_3 decreases, V tends to increase, with $V_{\max}$ occurring at $\theta_3 \in [-\pi/6, \pi/6]$.

3. Research on the influence of connecting rod parameters on motion flexibility

Common methods for constructing the Jacobian matrix include the differential transformation method and the vector product method. After comparison, it is found that the differential transformation method is simpler than the vector product method. This paper employs the differential transformation method to obtain the Jacobian matrix ($\boldsymbol{J}^*(\boldsymbol{\theta})$) of a manipulator. It should be noted that $\boldsymbol{J}^*(\boldsymbol{\theta})$ obtained by the differential transformation method is based on the end-

effector coordinate system of the manipulator. Therefore, it is necessary to transform it into $\boldsymbol{J}(\boldsymbol{\theta})$ relative to the base coordinate system using Eq. (3).

$$\boldsymbol{J}(\boldsymbol{\theta}) = \begin{bmatrix} {}^{0}_{n}\boldsymbol{R} & 0 \\ 0 & {}^{0}_{n}\boldsymbol{R} \end{bmatrix} \boldsymbol{J}^{*}(\boldsymbol{\theta}) \tag{3}$$

where ${}^{0}_{n}\boldsymbol{R}$ represents the orientation transformation matrix of the robotic arm's end-effector coordinate system relative to the base coordinate system.

Manipulability $\omega(\theta)$ [21] is important indicators for evaluating the flexibility of a manipulator. Both are defined based on $\boldsymbol{J}(\boldsymbol{\theta})$, and its calculations is shown in Eq. (4).

$$\omega(\theta) = \sqrt{\det(\boldsymbol{J}(\boldsymbol{\theta})\boldsymbol{J}^{T}(\boldsymbol{\theta}))} \tag{4}$$

The larger the value of $\omega(\theta)$, the more flexible a manipulator is, and vice versa. When $\omega(\theta) = 0$, the manipulator is in a singular configuration.

It should be noted that once the structure and dimensions of a manipulator are determined, $\omega(\theta)$ changes with the joint positions of the manipulator. This means that it is, in fact, only indicators of local flexibility.

To describe the global flexibility of a manipulator, the average manipulability $\bar{\omega}(\theta)$ is introduced, as shown in Eq. (5).

$$\bar{\omega}(\theta) = \frac{1}{V}\int_{\Omega} \omega_i(\theta)\mathrm{d}V_i \tag{5}$$

In the formula, Ω represents the range of a manipulator's workspace, $\omega_i(\theta)$ is the manipulability within the sub-space volumes divided from the manipulator's workspace, and V_i is the volume of the sub-space divided from the manipulator's workspace. The larger $\bar{\omega}(\theta)$, the better the global flexibility.

3.1 Analysis of the impact of link dimensions and link offsets on the global flexibility

Similar to Section 2, $a_1 = 20\text{mm}$, $a_2 = 50\text{mm}$, $a_3 = 50\text{mm}$, $d_5 = 100\text{mm}$, and $a_6 = 30\text{mm}$ are chosen. Further analysis of the changes in

$\bar{\omega}(\theta)$ as each link size and link offset varies from low to high is shown in Figure 4, leading to the following conclusions: (1) When a_1 and d_5 change, the manipulator's $\bar{\omega}(\theta)$ fluctuates around 19 and 18.3, respectively. The minor fluctuations are due to the randomness of joint position points during the Monte Carlo method for calculating the workspace. Therefore, these two parameters do not affect $\bar{\omega}(\theta)$. (2) Increasing the length of a_3 and a_6 uniformly results in a decrease in $\bar{\omega}(\theta)$, with almost the same degree of influence. At $a_2 = 50$, a local minimum appears. The reason for this may be that certain combinations of link lengths and joint angles cause some parts of the manipulator to interfere with each other, restricting the movement of the end effector in certain directions. It could also be that the manipulator requires greater force or torque to move in certain directions, thereby reducing its flexibility and efficiency. However, from a global perspective, an increase in the length of a_2 generally causes $\bar{\omega}(\theta)$ to increase, with its impact slightly higher than that of a_3 and a_6.

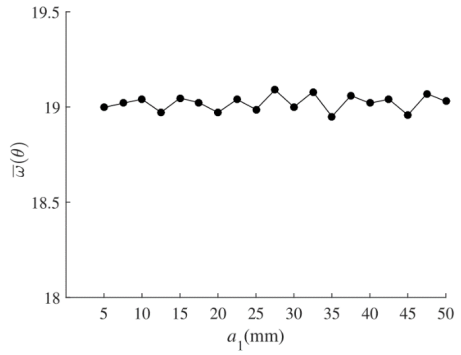

(a) The influence pattern of a_1 on $\bar{\omega}(\theta)$.

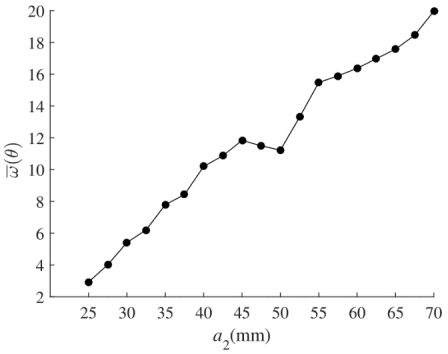

(b) The influence pattern of a_2 on $\bar{\omega}(\theta)$.

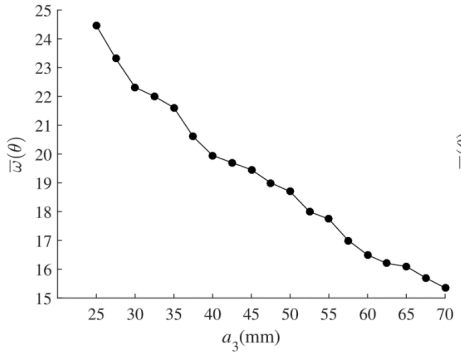

(c) The influence pattern of a_3 on $\bar{\omega}(\theta)$.

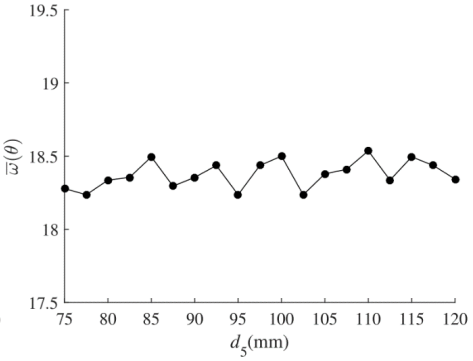

(d) The influence pattern of d_5 on $\bar{\omega}(\theta)$.

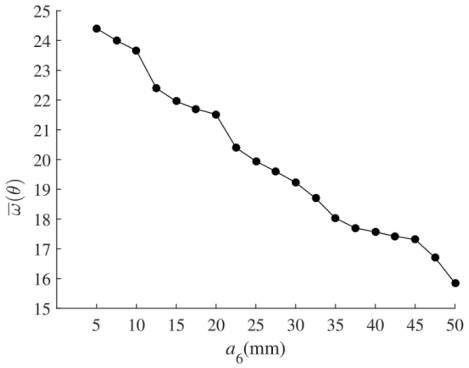

(e) The influence pattern of a_6 on $\bar{\omega}(\theta)$.

Fig. 4 Influence of connecting rod size and connecting rod offset on $\bar{\omega}(\theta)$

3.2 Analysis of the impact of joint position range on global manipulability

Each joint position range is changed one by one while the other joint position ranges remain constant. The changes $\bar{\omega}(\theta)$ as each joint position range varies are shown in Figure 5.

Observing Figure 3, the following conclusions are drawn: (1) When the range of the mobile joint d_1 changes, $\bar{\omega}(\theta)$ of the robotic arm fluctuates around 21. When the ranges of the rotating joints θ_5 and θ_7 change, $\bar{\omega}(\theta)$ of the manipulator fluctuates around 19.2 and 18.7, respectively. The reason for the small fluctuations is that the joint position points in the workspace are random during the Monte Carlo method, hence these three parameters do not affect $\bar{\omega}(\theta)$. (2) As the range of joint θ_2 decreases, $\bar{\omega}(\theta)$ tends to increase, and it is maximum at $\theta_2 \in [-\pi/6, \pi/6]$. (3) When the ranges of joints $\theta_{3\min}$ and $\theta_{6\min}$ decrease, and the ranges of joints $\theta_{3\max}$ and $\theta_{6\max}$ increase, $\bar{\omega}(\theta)$ tends to increase, thus $\bar{\omega}(\theta)$ is maximum for joints $\theta_3 \in [-\pi/6, \pi]$ and $\theta_6 \in [-\pi/6, \pi]$. (4) When the range of joint $\theta_{4\min}$ decreases, $\bar{\omega}(\theta)$ tends to increase; when the range of joint $\theta_{4\max}$ increases, $\bar{\omega}(\theta)$ first increases and then decreases, thus $\bar{\omega}(\theta)$ is maximum at $\theta_4 \in [-\pi/6, \pi/2]$

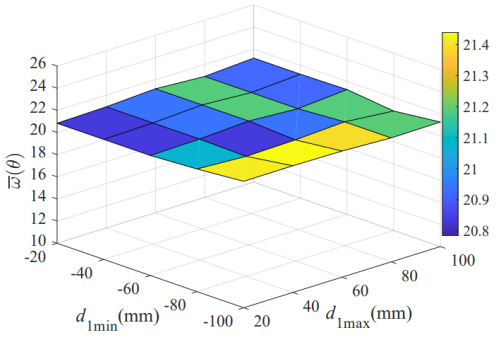

(a) The influence pattern of d_1 on $\bar{\omega}(\theta)$.

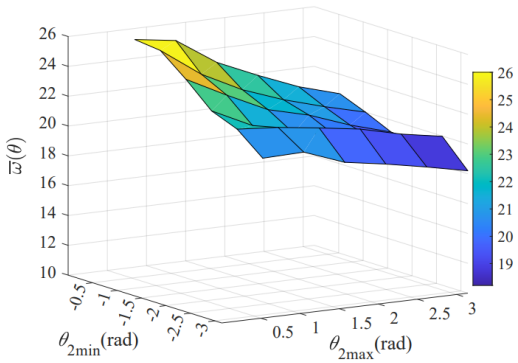

(b) The influence pattern of θ_2 on $\bar{\omega}(\theta)$.

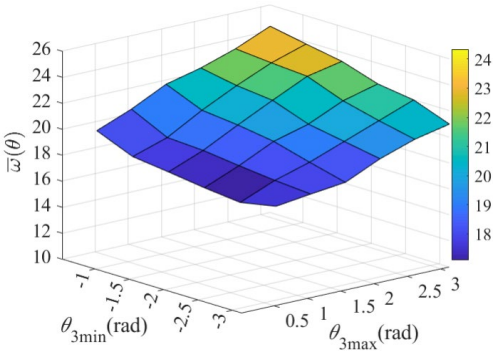

(c) The influence pattern of θ_3 on $\bar{\omega}(\theta)$.

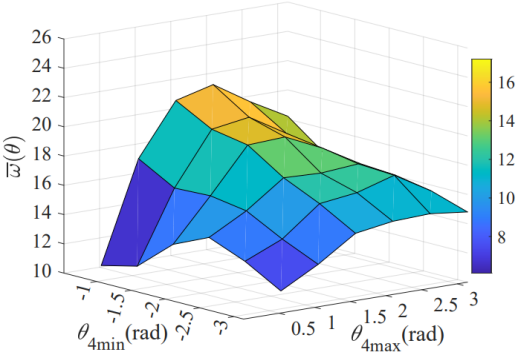

(d) The influence pattern of θ_4 on $\bar{\omega}(\theta)$.

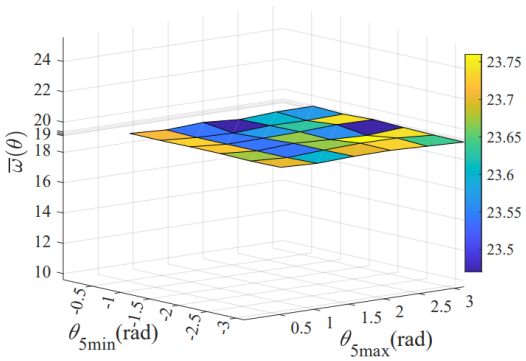

(e) The influence pattern of θ_5 on $\bar{\omega}(\theta)$.

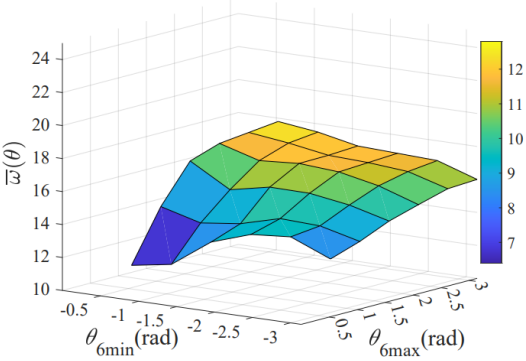

(f) The influence pattern of θ_6 on $\bar{\omega}(\theta)$.

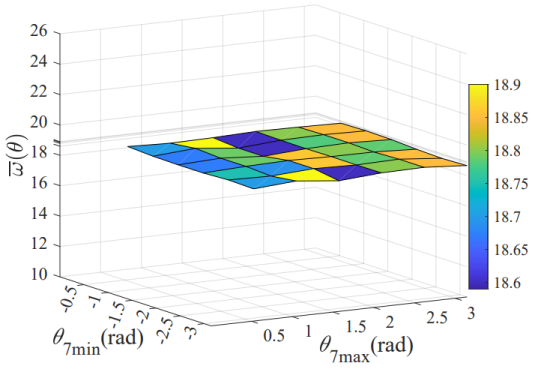

(g) The influence pattern of θ_7 on $\bar{\omega}(\theta)$.

Fig. 5 Influence of range variation of joint position on $\bar{\omega}(\theta)$

4. Parameter optimization of connecting rod of the 7 DOF manipulator

After completing the structural design of the 7 DOF manipulator, it is necessary to optimize the parameters of its links. The goal is to achieve a larger workspace and better control performance without changing the total length of manipulator. To this end, the optimization of link parameters is carried out with V and $\bar{\omega}(\theta)$ as the objective functions.

$$\begin{cases} \text{Max} & f_1(\hat{x}) = \bar{\omega}(\theta) \\ \text{Max} & f_2(\hat{x}) = V \end{cases} \tag{6}$$

As can be seen from Figures 2 and 4, a_1 does not affect V or $\bar{\omega}(\theta)$. Therefore, set a_1 = 20mm and no longer consider it as a variable for optimization. With the constraint that the total length of the link parameters of the manipulator in the state of Figure 1(a) remains unchanged and there are no voids in the workspace. Additionally, considering the control of the end-effector pose and the assembly of the manipulator's links, as well as the impact of link parameters on V or $\bar{\omega}(\theta)$, constraints are also needed for the link parameters. The ranges of d_1, θ_5, and θ_7 do not affect V or $\bar{\omega}(\theta)$ of the 7DOF manipulator; thus, these three link parameters also do not need to be optimized. At this point, the matrix of parameters to be optimized, $\hat{x}$ is represented by Eq. (7):

$$\hat{\boldsymbol{x}} = [\theta_{2\min},\ \theta_{2\max},\ \theta_{3\min},\ \theta_{3\max},\ \theta_{4\min},\ \theta_{4\max},\ \theta_{6\min},\ \theta_{6\max},\ a_2,\ a_3,\ d_5,\ a_6]^{\mathrm{T}} \tag{7}$$

In summary, the optimization function for the link parameters of the 7DOF manipulator encompasses two sub-objectives and involves optimizing 12 parameters, which constitutes a multi-variable and multi-objective optimization problem. To enhance optimization efficiency, this problem is transformed into a single-objective optimization problem. Concurrently, weight coefficients and scaling factors for the objective functions are introduced. The final optimization model is represented by Eqs. (8) to (9):

$$\text{Max } f(\hat{x}) = \eta_1 \frac{f_1(\hat{x})}{s_1} + \eta_2 \frac{f_2(\hat{x})}{s_2} \tag{8}$$

$$\text{s.t.} \begin{cases} -\pi \le \theta_2 \le \pi \\ -\pi \le \theta_3 \le \pi \\ -\pi \le \theta_4 \le \pi \\ -\pi \le \theta_6 \le \pi \\ 25\text{mm} \le a_2 \le 70\text{mm} \\ 25\text{mm} \le a_3 \le 70\text{mm} \\ 75\text{mm} \le d_5 \le 120\text{mm} \\ 20\text{mm} \le a_6 \le 30\text{mm} \\ a_2 + a_3 + d_5 + a_6 = 230\text{mm} \\ |d_5 - a_6| \le |a_2 + a_3| \le |d_5 + a_6| \end{cases} \tag{9}$$

where η_1 and η_2 are the weight coefficients of the objective functions, and s_1 and s_2 are the scaling factors. To ensure that the manipulator can flexibly and efficiently complete complex movements, the global manipulability objective is more important than the workspace volume. By further comparing the orders of magnitude of V or $\bar{\omega}(\theta)$ as the link parameters change in Figures 2 to 5, the values of $\eta_1 = 0.6$, $\eta_2 = 0.4$, $s_1 = 18$, and $s_2 = 3.6\times10^7$ are ultimately determined.

The PSO algorithm is employed to solve for and normalize the optimized parameters, with the results presented in Table 2. The sum of the joint variables is calculated, and the pre- and post-optimization link parameters are substituted into

the kinematic model. The corresponding V or $\bar{\omega}(\theta)$ are calculated using Eqs. (1) and (5), with the results displayed in Table 3. The results indicate a 25.694% reduction in the sum of joint variables, an 8.696% increase in the workspace volume, and an 8.824% increase in average manipulability, suggesting that the optimized robotic arm has a larger workspace and more flexible movement.

Table 2

Comparison of connecting rod parameters before and after optimization

Link Parameters	θ_2 (rad)	θ_3 (rad)	θ_4 (rad)	θ_6 (rad)	a_2 (mm)	a_3 (mm)	d_5 (mm)	a_6 (mm)
Before Optimization	$[-\pi, \pi]$	$[-\pi, \pi]$	$[-\pi, \pi]$	$[-\pi, \pi]$	50	50	100	30
After Optimization	$[-\pi, 5\pi/6]$	$[-\pi/6, \pi]$	$[-2\pi/3, \pi]$	$[-5\pi/18, \pi]$	68	32	110	20

Table 3

Comparison of indicators before and after optimization

Optimization Metrics	$f(\bar{x})$	V (mm^3)	$\bar{\omega}$	Sum of Joint Variables (rad)
Before Optimization	1.078	4.6×10^7	17	8π
After Optimization	1.172	5.0×10^7	18.5	$107\pi/18$
Optimization Percentage %	+8.720	+8.696	+8.824	– 25.694

Note: "+" indicates an increase or improvement, " – " indicates a decrease or reduction

5. Conclusions

An optimization method for the link parameters of a manipulator is proposed. First, the average manipulability is introduced as a global flexibility evaluation index for the manipulator. The influence of link parameters on the workspace volume and average manipulability of a 7-DOF manipulator is analyzed respectively, which helps to determine the link parameters that do not need optimization. Further, with the link parameters and the absence of voids in the workspace of the 7-DOF manipulator as constraints, and the workspace volume and average manipulability as optimization objectives, an optimization model is established. By introducing the weight coefficients and scaling factors for the objective functions, the multi-objective problem is transformed into a single-objective problem, and the PSO algorithm is employed to solve for the

optimal link parameters. The results show that after optimization, the total sum of joint variables was reduced by 25.7%, the workspace volume increased by 8.696%, and the average manipulability increased by 8.824%. This indicates that the optimized manipulator has a larger workspace and more flexible movement. Thus, the rationality of the optimization method is verified, and a theoretical basis for manipulator design and flexibility analysis is provided.

Acknowledgments

This work was supported by the Jiangsu Ocean University Haizhou Bay Talent Innovation Fund (under Project No. KQ24024).

R E F E R E N C E S

[1]. *Q. Y. Zhang, Y. Zhang, H. R. Chen, et al.* "Workspace and singularity analysis of desktop 607 manipulator", Agricultural equipment and vehicle engineering, **vol. 60**, no. 9, Sep. 2022, pp. 37-42.

[2]. *W. N. Hu*. "Optimization of arm length parameters for PUMA robots based on workspace", Robot Technique and
Application", Robot Technique and Application, **vol. 200**, no. 2, Feb. 2021, pp. 23-27.

[3]. *T. M. Chen, Z. L. Yao, J. Zhang.* "The workspace computation of aerial platform truck based on Monte-Carlo method", Construction Machinery, **vol. 2**, no. 528, Jul. 2020, pp. 57-61.

[4]. *X. D. Jing, Q. Y. Xue, N. Y. Chen.* "Analyzing and Optimizing Parameters of 6R Dual-arm Service robot Collaborative Space", Mechanical Science and Technology for Aerospace Engineering, **vol. 40**, no. 6, June. 2021, pp. 840-845.

[5]. *Q. C. Feng, C. Ji, J. W. Zhang, et al.* "optimization design and kinematic analysis of cucumber -harvesting-robot manipulator", Transactions of the Chinese Society for Agricultural Machinery, **vol. 44**, no. S1, 2010, Sep. pp. 244-248.

[6]. *F. C. Yin, H. W. Shi, Q. Z. Ji, et al.* "Analysis and optimization for kinematic performance of stone-craving robotic manipulators", Machine Tool and Hydraulics, **vol. 50**, no. 9, May. 2022, pp. 24-34.

[7]. *X. J. Lan, X. D. Li.* "Research on Optimization of Motion Characteristics of a Parallel Robot Mechanism", Machine Tool and Hydraulics, **vol. 51**, no. 8, Apr. 2023, pp. 80-88.

[8]. *Q. Meng, Z. Jiao, H. Yu, et al.* "Design and evaluation of a novel upper limb rehabilitation robot with space training based on an end-effector", Mechanical Sciences, **vol. 12**, no. 1, Dec. 2021, pp. 639-648.

[9]. *R. P. Paul, C. N. Stevenson.* "Kinematics of robot wrists", The International Journal of Robotics Research, **vol.**, no. 2, 1983, pp. 31-38.

[10]. *J. K. Salisbury, J. J. Craig.* "Articulated hands: force control and kinematic issues", The International Journal of Robotics Research, **vol. 1**, no. 1, Mar. 1982, pp. 4-17.

[11]. *L. T. Yu, J. Yang, L. Wang, et al.* "Dexterity-based optimization of dimension and structure for a surgical robot", Journal of Harbin Engineering University, **vol. 38**, no. 12, Dec. 2017, pp. 1943-1950.

[12]. *R. V. Mayorga, J. Carrera, M. M. Oritz.* "A kinematics performance index based on the rate of change of a standard isotropy condition for robot design optimization", Robotics and Autonomous Systems, **vol. 53**, no. 3, Dec. 2005, pp. 153-163.

[13]. *H. Dong, W. T. Wu, H. Sun.* "Dimension Optimization of Manipulator Based on Workspace Density Function", Machine Building and Automation, **vol. 48**, no. 5, Oct. 2019, pp. 143-146.

[14]. *Z. Y. Zhao, Z. B. Xu, J. P. He, et al.* "Configuration Optimization of Nine Degree of Freedom Super-redundant Serial Manipulator Based on Workspace Analysis", Journal of mechanical engineering. **vol. 55**, no. 21, Nov. 2019, pp. 51-63.

[15]. *X. H. Li, X. S. Shi, L. Lv, et al.* "Size Optimization Method of 6R Manipulator Based on Global Maneuverability", Journal of System Simulation, **vol. 31**, no. 12, Dec. 2019, pp. 2569-2574.

[16]. *D. Liang, Z. Y. Liang, B. Y. Chan, et al.* "Optimal design of assisting-riveting parallel robot for lifting arm of dobby loom", Chinese Journal of Engineering Design, **vol. 29**, no. 1, Feb. 2022, pp. 28-40.

[17]. *B. Hu.* "Performance analysis and optimization research of spinal puncture robot based on parallel mechanism", Shanghai Jiao Tong University, 2021. DOI: 10.27307/d.cnki.gsjtu.2021.000180.

[18]. *X. H. Yang, Z. Y. Zhao, Y. T. Li. et al.* "Inverse Kinematics Solution of Redundant Manipulator Based on Manipulability Optimization", Journal of mechanical engineering, **vol. 60**, no. 7, Apr. 2024, pp. 22-33.

[19]. *Z. Y. Liao, B. Chen, Q. Zheng. et al.* "Collaborative workspace design of supernumerary robotic limbs base on multi-objective optimization", Journal of the Brazilian Society of Mechanical Sciences and Engineering, **vol. 45**, no. 7, Feb. 2023, pp. 354-367.

[20]. *X. L. Zhang, Y. Xu, S. Xu. et al.* "Volume analysis and void-free design of the workspace of a 7 DOF manipulator", University Politehnica of Bucharest, Scientific Bulletin, Series D: Mechanical Engineering, **vol. 92**, no. 4, Dec. 2024, pp. 19-30.

[21]. *T. Yoshikawa.* "Manipulability of robotic mechanisms", The International Journal of Robotics Research, **vol. 4**, no. 2, Jun. 1985, pp. 3-9.